TESTING OF ADAPTIVE AIRFOIL FOR UAV USING SHAPE MEMORY ALLOY ACTUATORS

Ermira J. Abdullah, Cees Bil and Simon Watkins
School of Aerospace, Mechanical and Manufacturing Engineering, Royal Melbourne Institute of Technology, Melbourne, Australia.

Keywords : *adaptive airfoil, shape memory alloy, uav*

Abstract

Adaptive airfoil control system can potentially improve flight performance by optimizing the maximum lift-to-drag ratio throughout all flight regimes. Improved flight performance translates into weight and fuel savings.

Smart material is a suitable candidate for adaptive airfoil design as it can be activated to alter the shape of the airfoil. One such material is the Shape Memory Alloy (SMA). It is lightweight, produces high force and large deflection which makes it a perfect choice for actuator in the adaptive airfoil system design.

The deflection of a variable cambered wing is controlled by means of resistive heating of SMA actuators and cooling in the surrounding air. Finite element analysis (FEA) was used to design a flexible wing and based on the FEA result an experimental wing model was fabricated to test the application of the SMA actuators. The SMA actuators were fixed underneath the wing skin. The heating of the wires caused them to contract, creating a force and generating a moment which deflects the wing. Static experiment was carried out to compare with the FEA simulation.

A wind tunnel test was performed to investigate the change in lift to drag ratio of the wing when the actuator is switched on and off. The results proved that the use of SMA actuators in the wing model is reliable as significant change in lift to drag ratio was detected when the wing morphed.

1 Introduction

UAV which utilizes adaptive airfoil control system is able to improve its aerodynamics performance. In order to obtain optimum performance it is necessary that UAV cruises close to the best lift to drag ratio (L/D) [1] which means flying at constant angle of attack. In order to maintain flying at the best L/D may require a climbing cruise because weight decreases due to fuel consumption. This is usually not desirable because of flight or air traffic control restrictions. Finding a balance between weight, altitude, speed and/or wing area is crucial because a failure to do so may cause the L/D to be lower than the best L/D and the range will be correspondingly less. Variable camber wing may provide a solution to this predicament. Adaptive airfoil control allows the UAV to change its lift coefficient during cruise in order to operate at optimum L/D for any given lift coefficient and at constant angle of attack. An analytical study conducted by NASA [2] on the benefits of variable-camber capability revealed that drag can be significantly reduced if all wing trailing edge surfaces are available for optimization such as in the case of flight with variable camber capability. The main aerodynamic benefits of variable camber airfoil are increase of aerodynamic efficiency (L/D ratio) by up to 9%, extended buffet boundaries by up to 15% and reduction of wing root bending moments by up to 12%.

Due to the potential benefits of employing adaptive airfoil, there has been an intensive attempt by researchers in developing a working model. With the advancement of materials, many are now considering using smart materials to produce airfoil with variable camber capability. Smart material actuators are light and they take up less space compared to conventional actuators which are bulky and heavy. One of the most popular choices of

smart material is shape memory alloy. It comes in the form of wire, rod and also spring.

Shape memory alloy spring has been used as an actuator for an adaptive airfoil [3]. SMA springs with the help of stop structures are used to actuate accurately certain points on the skins to approach the target airfoil. From the simulation and measured results, it was discovered that the skin actuated by SMA springs on specific discrete points could obtain good actuating results near these points. There were errors between simulation value, measured value and target value, at the positions far away from the points actuated. The error was the biggest at points which are far away from both the actuated points and the constraint points, caused by the difference between the successive deformation character of rigid body and the singular character of the target shape. This means average distribution of actuated points along the chord was favorable to approach the target shape better.

Hutapea et al [4] has developed a prototype of a smart actuation system for an adaptive airfoil by controlling the flaps. SMA springs were fixed at one end to the wing box toward the leading edge of the airfoil while the other end was attached tangentially to a rotating cylinder fixed to the flap. In order to produce rotation of the flap in both the upward and downward directions, the springs were arranged in an upper and a lower layer. An applied current was used to produce heat which controlled the spring actuators. The prototype developed demonstrated strong potential for future application based on the experimental and theoretical analysis.

Another method of changing the airfoil shape [5] is by moving the transition point position on the airfoil using a single point control as proposed by Popov et al. SMA actuator was used to move the transition point closer to the leading edge in order to improve the laminar flow on a wing. The upper surface of the airfoil was modified using an actuator located at a certain percentage of the chord where its corresponding deflection was obtained. The transition point positions were found from the detection of sudden increase of pressure.

Strelec et al [6] has examined the feasibility of using SMA actuator in a reconfigurable airfoil. Structural and aerodynamics analyses were carried out on an experimental wing model that was developed. From the bench test it was clear that the SMA actuators were effective in producing a camber change as the trailing edge deflection measured 6.0 mm. The results from the wind tunnel test showed an increase in the lift coefficient at 0, 5 and 10 degrees angle of attack, when the SMA actuators were turned on. However, the effect on lift to drag ratio can't be determined because the change in drag coefficient was not presented.

The objective of this research is to develop an adaptive airfoil control system using shape memory alloy actuator which will be implemented on a UAV. This paper describes the feasibility of implementing an adaptive airfoil control system for a typical Unmanned Aerial Vehicle (UAV) wing, focusing on the characteristics of aerodynamic and structure. The aim is to investigate the reliability of using the SMA actuators in producing change in the airfoil camber. The deflection produced by the SMA actuators was found using a static experiment and the result is compared with the FEA simulation. The effect on the performance can be determined by analyzing the lift to drag ratio of the wing before and after the actuator was switched on.

2 Shape Memory Alloy as Actuator

Smart material can be tailored to create a specific response to a combination of inputs [7]. These materials include piezoelectrics and electrostrictives, and shape memory alloy. In the case of adaptive airfoil, Fontanazza et al [8] concluded that the ideal material should respond quickly to external stimuli, be capable of large and recoverable free strains, transform effectively the input energy to mechanical energy, and not be affected by fatigue issues. They suggested that the benefits of using smart material compared to pneumatic or hydraulic actuators are reduced complexity and improved reliability of the system.

Table 1 [9] lists the most common characteristics of some smart materials which include maximum free strain, maximum stress, deformation energy density, efficiency, and relative speed of response. Among all the smart materials, SMAs appear to have superior capability in producing large plastic deformations. In recent years, interest in SMAs applications for adaptive structures have been increasing not only due to this unique quality, but also because of their high power-to-weight ratio and low driving voltages. SMAs are thermomechanical materials [7] typically comprise of a mixture of nickel and titanium, which changes shape when heated or cooled. When they are cooled to below a critical temperature their crystal structure enters the martensitic phase, where alloy is plastic and can easily be manipulated through very large strain ranges with little change in the material stress. However, when heated, above the critical temperature, the phase changes to the austenitic phase, where the alloy resumes the shape that it formally had at the higher temperature.

Table 1 The Characteristics of Smart Materials.

Material	Max. strain (%)	Max. stress (MPa)	Elastic energy density(J/g)	Max. effic. (%)	Relative speed
Electrostrictor Polymer P (VDF-TrFE)	4	15	0.17	-	Fast
Piezoelectric Ceramic (PZT)	0.2	110	0.013	>90	Fast
Single Crystal (PZN-PT)	1.7	131	0.13	>90	Fast
Polymer (PVDF)	0.1	4.8	0.0013	n/a	Fast
SMA (TiNi)	>5	>200	>15	<10	Slow

Nickel titanium is the most commonly used SMA to which copper is sometimes added to aid in the strain recovery process. The process of shape change or creating movement comprise of a five-step procedure that occurs within the material in which the shape memory effect is developed. Fig. 1 shows the entire process [10,11]. The first step is the parent austenitic phase which occurs at a high temperature with zero stress and strain. In order to create twinned martensite, the parent austenitic structure is cooled in the absence of both stress and strain. Next, the twinning process is reversed by stressing the material which causes the now detwinned martensite to develop inelastic strains. While still maintaining its detwinned form with the elastic strain, the load is then released. Finally, the material returns to its original shape and composition when all inelastic strains are recovered by heating the SMA to its parent austenitic start temperature.

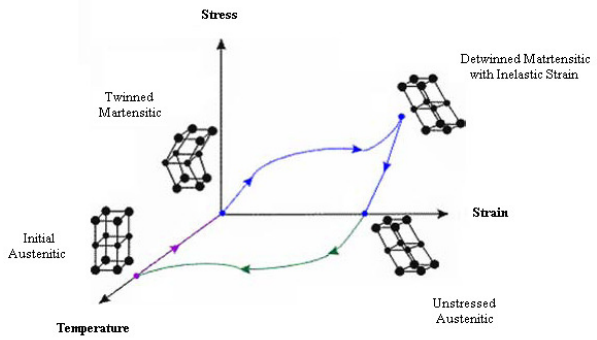

Fig. 1 Schematic of Temperature-Stress-Strain [10,11] for SMA Crystallographic Phase Transformation.

3 Experimental Model

FEA was used to predict the effectiveness of the SMA actuator. Different configurations were analyzed by changing the skin material, the position of the SMA actuators within the wing and forces exerted by it on the skin. In the simplified 3D FEA model which is shown in Fig. 2, a structural static simulation of the wing panel deformation was considered with the SMA actuators action incorporated as concentrated forces.

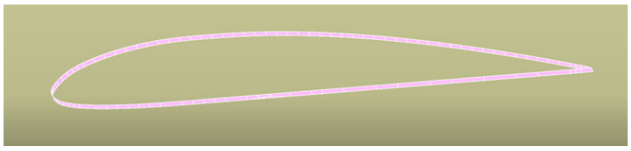

Fig. 2 Simplified FEM Model of the Wing Panel

In the FEM model the wing panel was represented as wing skin with the spar, ribs, base and solid leading edge was built-in as boundary conditions. Clark Y airfoil was used with a chord of 1 m. The span was 0.01 m and the thickness of the skin was 4 mm. The skin thickness was chosen such that the airfoil is able to deform while minimizing the occurrence of buckling. Plywood, aluminum and acrylonitrile butadiene styrene plastic (ABS) were analyzed

for the wing skin. It was possible to position the actuator in various ways. Given that shape memory alloy wires will be used, a truss configuration can be implemented as they only provide tension forces.

Placement of the actuator is critical in obtaining the desired change of the airfoil camber. Different combinations of applied forces by the SMA actuators were analyzed. The actuators were attached to two points near the leading edge of the airfoil. The coordinates of the points were (0.17, 0.08) and (0.35, -0.03). An example of result from the FEM analysis is shown in Fig. 3. The deformation effectively created a camber across the airfoil. The analyses were repeated for different types of wing skin material with significant variation in trailing edge deflection. Wing panel with ABS skin produces the biggest trailing edge deflection for the same forces applied by the SMA actuators and wing panel with aluminum skin produces the smallest deflection.

Fig. 3 Morphing of Wing Panel When the SMA Wires are Fully Actuated

A wing model was then fabricated. The prototype has a span of 175 mm and its chord is 247 mm. The airfoil is a Clark Y which has a flat base. Choosing a suitable material for the skin is critical in order to get a significant change in camber while maintaining the airfoil shape. ABS was selected as the skin material based on the results of the FEA analyses. It is a durable, high strength modeling material that can be machined, sanded, drilled, painted and glued after the model is built. It was used in the second generation prototype wind tunnel model for reconfigurable wing at Texas A&M University College Station [6]. In order to produce the most desirable result, it was critical that the skin thickness was minimized. The model was successfully fabricated with a 1 mm skin thickness using a rapid prototyping machine. However, the span was reduced from what was initially plan due to warping of the wing when the span was too long. This was probably caused by the very thin skin.

The wing was actuated by SMA wires at the leading edge. The SMA wires used in this model were FLEXINOL® wire actuators produced by Dynalloy Inc. The wires were 0.3048 mm in diameter, 35 mm in length and were precrimped with ring crimps. Nine actuators which consist of four parallel wires each were connected in series. In total, 36 SMA wires were used. The SMA wires were arranged inside the wing in a series configuration on two pieces of wood and attached to the wing's leading edge. No actuators were placed near the trailing edge due to space constraints. The wing model is shown in Fig. 4.

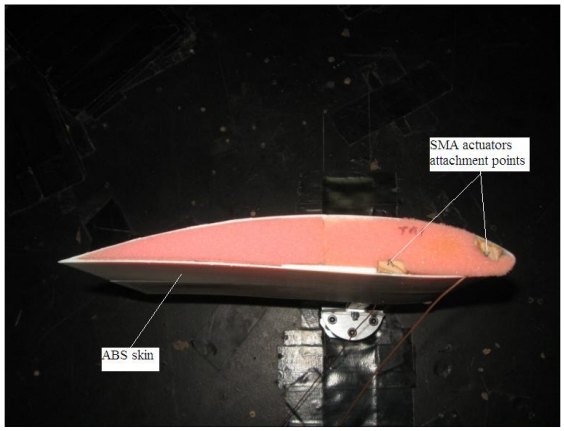

Fig. 4 Side View of the Experimental Wing Model

A static experiment was conducted to test the capabilities of the SMA actuators. When they were fully actuated, it caused the airfoil to deform and produced a change in the airfoil camber. The deflection of the trailing edge was measured to be approximately 6 mm, which is the same as the one produced by the morphing wing developed by Strelec et al [6]. FEA predicted a deflection of approximately 9 mm at maximum force for the same SMA actuator. The smaller deflection in the experiment was probably due to the amount of current used was not enough to produce maximum force. This was done on purpose to avoid overloading the SMA actuator.

As anticipated there were a few drawbacks in using the SMA wire actuators. The most

obvious is the slow rate of cooling which consequently affected the performance of the actuators. The first test produces the biggest deflection and the trailing edge deflection reduces after a few tests. In order to get a relatively constant result, the actuators had to be given enough time to cool down completely. Another downside is the high energy consumption of the actuators. Initially batteries were used but it proved to be expensive as they drained the batteries fairly quickly. To overcome this problem, the batteries were replaced by dc voltage source.

4 Influence of Airfoil Shape on Flight Performance

Lift coefficient (C_L) and drag coefficient (C_D) are complex functions of profile shape, angle of attack (α), wing planform (S) Mach number (M) and Reynolds number (Re), which can be defined as

$$C_L = L/qS \qquad (1)$$

$$C_D = D/qS \qquad (2)$$

and

These functions may be obtained from computation, wind tunnel testing or flight testing. The aerodynamic results are usually presented as graphs of

$$C_L = f(\alpha) \qquad (3)$$

$$C_D = f(\alpha) \qquad (4)$$

and

$$C_D = f(C_L) \qquad (5)$$

Typical curves of these functions for low-speed (no shock wave) flight are shown in Figs. 5 - 7. It can be seen from the graphs that the curves of Eqns. (4) and (5) have parabolic shape in the region where the C_L variation with α is approximately linear.

The maximum achievable lift to drag ratio (L/D) in cruise flight is a very important performance parameter. It can be defined as

$$L/D = C_L/C_D \qquad (6)$$

It can be plotted as a function of C_L as shown in Fig. 8. In performance optimization, L/D is maximized for all flight cruise conditions.

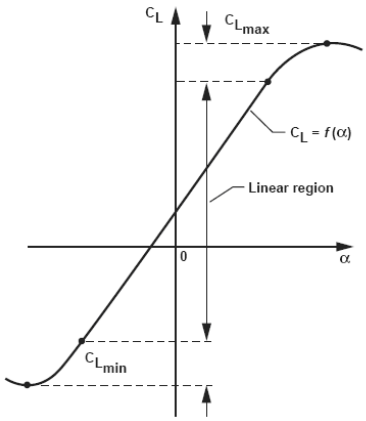

Fig. 5 Change of Lift Coefficient with Angle of Attack [2] .

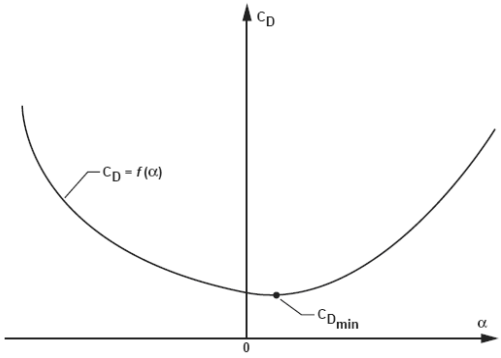

Fig. 6 Change of Drag Coefficient with Angle of Attack [2].

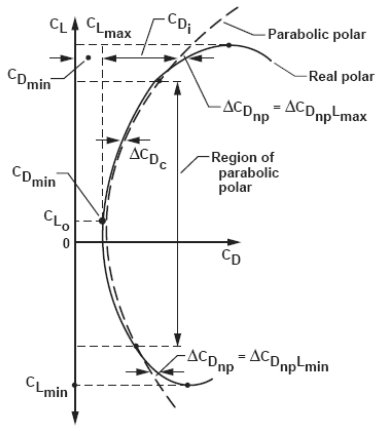

Fig. 7 Schematic of a Typical Polar of an Aircraft [2].

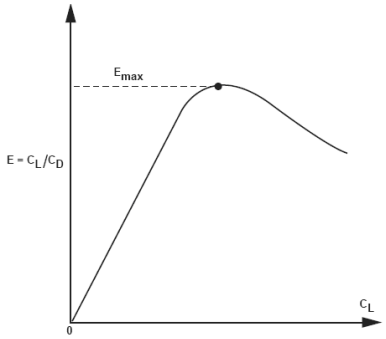

Fig. 8 E = C_L/C_D as a Function of Lift Coefficient [2].

The change in camber produces varying effect on the aerodynamic performance depending on the modification. In the subsonic region, as camber increases, less α is required for a fixed C_L, or C_L increases for a constant angle of attack [12]. Increasing camber also increases the linear region of C_L as a function of angle of attack, to a larger C_L and the maximum C_L:

$$C_{L_{\max}}(\delta) = C_{L_{\max}}(\delta = 0) + \Delta C_{L_{\max}}(\delta) \qquad (7)$$

The minimum C_D increases by the relation:

$$C_{D_{\min}}(\delta) = C_{D_{\min}}(\delta = 0) + \Delta C_{D_{\min}}(\delta) \qquad (8)$$

The lift to drag ratio also has a significant effect on a UAV flight range [1] as given in the Breguet equation

$$Range = \frac{V}{c}\frac{C_L}{C_D}\ln\frac{W_0}{W_1} \qquad (9)$$

where V is the velocity, c is a constant, W_0 is the take off weight and W_1 is the landing weight. Since C_L/C_D is directionally proportional to the range, an increase in the C_L/C_D will cause the range of the UAV to increase.

5 Wind Tunnel Results and Discussions

The objective of the wind tunnel tests was to measure the lift force and drag force over the original and morphed airfoil shapes to verify that there is an increase in the lift to drag ratio when the SMA actuators are turned on. The RMIT Wind Tunnel was used to measure the aerodynamic properties of the flexible wing which is a closed return circuit wind tunnel with a maximum speed of approximately 150 km/h. The rectangular test section dimensions are 3 m (wide) x 2m (high) x 9 m (long) equipped with a turntable to yaw the sample under test. A plan view of the tunnel is shown in Figure 9 [13]. The mounting strut (sting) holding the flexible wing was mounted on a six component force sensor (type JR-3), and the purpose made computer software was used to determine all 6 forces and moments (drag, side and lift forces, and yaw, pitch and roll moments) and their non-dimensional coefficients.

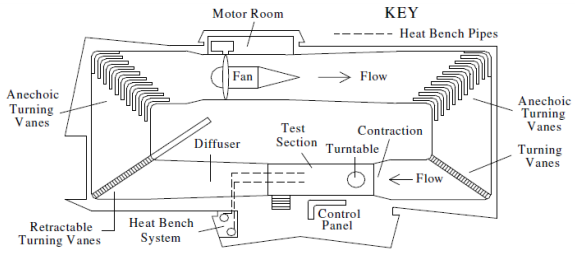

Fig. 9 A Plan View of RMIT University Wind Tunnel [13].

The model was subjected to flow with Reynolds number 146500, 195340, 244170 and 293000. The model was swept through 0, 5, and 10 degrees angle of attack. For each test case, data was taken for the original configuration. Then, the actuators were switched on and data was taken for the morphed configuration.

Firstly, the lift coefficients for both the original and morphed configuration are analyzed. This is due to data obtained by other researchers are available for comparison. Fig. 10 shows the lift coefficient plotted against angle of attack at Reynolds number 293000.

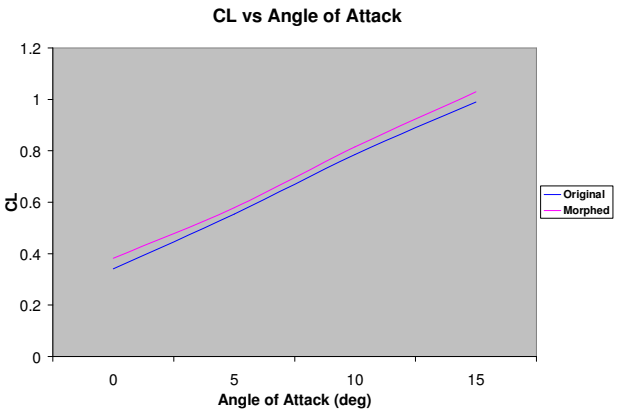

Fig. 10 Lift Coefficient at Re = 293000

From Fig. 10 it can be clearly seen that the lift coefficient for the wing was higher when it was morphed. The change in lift coefficient increases with angle of attack. This proves there is a change in the camber when the SMA actuators were switched on. It is appropriate to note that the data scatter in the experimental determination of the coefficient lift coefficients over the angle of attack for the model is not large, which points to a fairly high accuracy of the measurement.

The change in lift coefficient between the original and morphed configuration was calculated. The results are shown in Table 2.

Table 2 Change in Lift Coefficient Due to SMA Actuation

Angle of Attack	ΔC_L
0	0.041
5	0.025
10	0.030

The biggest increase of lift coefficient is by 0.041 at 0 degree angle of attack and the smallest increase in lift coefficient is by 0.025 at five degrees angle of attack. The increase in lift coefficients are comparable to those obtained by other researchers. For example, Strelec et al [6] observed the greatest improvement in lift coefficient is at zero degrees angle of attack, with an increase of about 0.062, based on SMA-actuated leading edge and trailing edge airfoil deflection. At five and ten degrees angle of attack, increases of 0.045 and 0.055, respectively, were detected.

However, an increase in lift coefficient does not necessarily translate into improved performance. The drag coefficient has to be taken into consideration in order to prove that the morphed configuration produces better result. When it comes to designing a wing, the greatest performance indicator is typically the lift to drag ratio. So it is essential that the lift to drag ratio is analyzed to determine the effects of using the SMA actuators on the deformable wing. Figs. 11 – 14 show the lift to drag ratio plotted against lift coefficient at Reynolds number 146500, 195340, 244170 and 293000.

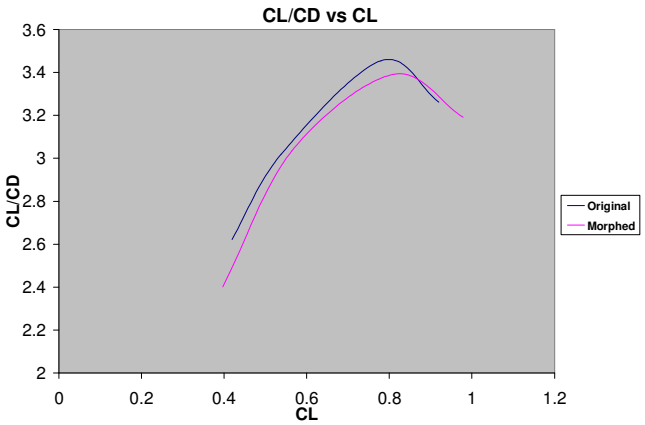

Fig. 11 C_L/C_D at Re = 146500

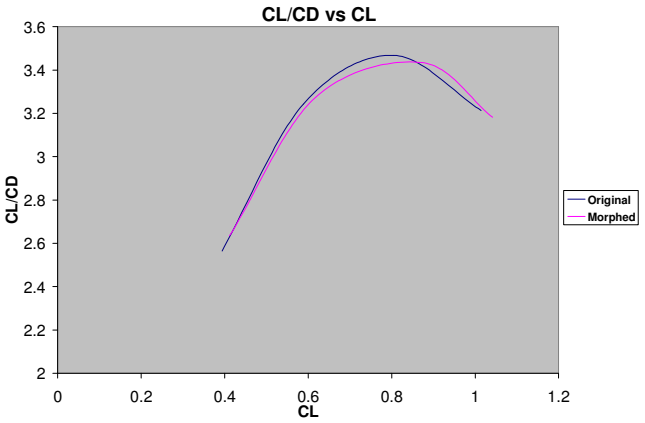

Fig. 12 C_L/C_D at Re = 195340

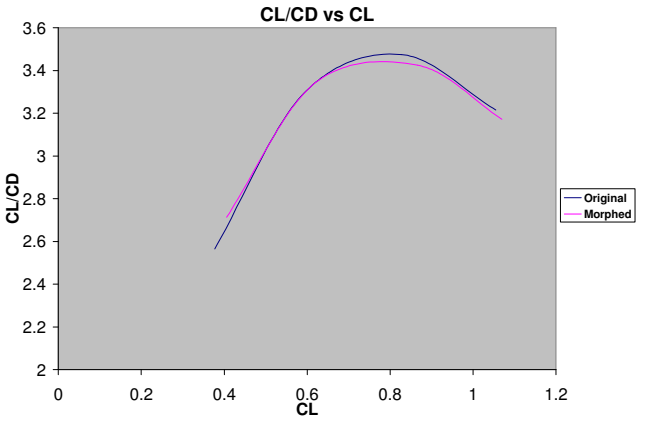

Fig. 13 C_L/C_D at Re = 244170

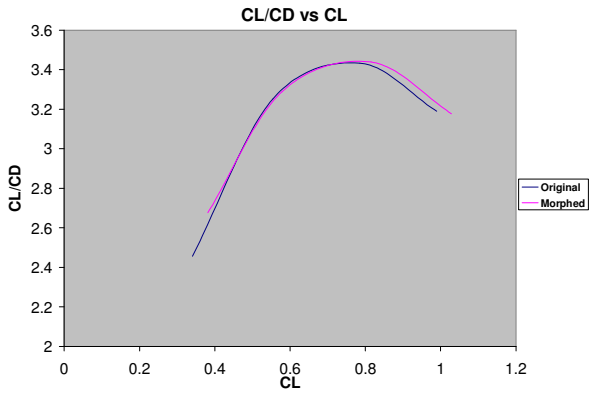

Fig. 14 C_L/C_D at Re = 293000

The lift to drag ratio for the morphed configuration is typically higher compared to the original configuration at high lift coefficient. At Reynolds number 293000, $(C_L/C_D)_{max}$ for the morphed configuration is higher than that of the original configuration. Increase in C_L/C_D translates into better flight range for UAV based on Eqn. (9).

The range of C_L for a typical UAV flight [14] may vary from 0.5 to more than 1.2. Fig. 14 shows that C_L/C_D for the morphed configuration is higher for C_L greater than 0.7, thus any UAV with a C_L greater than 0.7 would be able to benefit from utilizing morphing wings as they give a better C_L/C_D value. Since the weight of UAV decreases with time as fuel is consumed, the lift coefficient also decreases. It can obtain better performance by flying with morphed wing configuration at higher C_L and switching to the original wing configuration at lower C_L.

The effect of adaptive airfoil at different Reynolds number is compared in Table 3. The increase in C_L/C_D is significantly bigger at higher Reynolds number. At 0 degree angle of attack, when the SMA actuator was switched on, C_L/C_D increased by up to 8.97% at Reynolds number 293000. At 5 degrees angle of attack, C_L/C_D increased by up to 1.48% at Reynolds number 244170.

Table 3 Increase (%) in C_L/C_D

AOA	Re =146500	Re =195340	Re =244170	Re =293000
0	n/a	2.78	5.8	8.97
5	0.51	0.96	1.48	1.18

6 Conclusions

FEA was used to design a deformable wing model. A prototype was fabricated using ABS material for the skin and integrated with SMA actuators. The fabrication of the wing itself was a challenging task. A different manufacturing technique to produce a wing with ABS skin while minimizing the skin thickness could be explored. The performance of the SMA actuator might be improved by employing a controller to compensate for the hysteresis.

The deflection of a variable cambered wing was controlled by means of resistive heating of SMA actuator and cooling in the surrounding air. The SMA actuators were fixed underneath the wing skin near the leading edge. The heating of the wires caused them to contract, creating a force and generating a moment which deflected the wing. Static experiment was conducted and the results showed there is a trailing edge deflection of 6 mm which is comparable to that obtained through FEA.

Wind tunnel tests were performed to obtain experimental lift force and drag force data over the original wing shape and the morphed wing shape. Increase in lift coefficient was observed when the wing was morphed which indicates the successful implementation of the SMA actuated wing model in wind tunnel conditions. The biggest increase of lift coefficient is by 0.041 at 0 degree angle of attack and the smallest increase in lift coefficient is by 0.025 at five degrees angle of attack. The increase in lift coefficients are comparable to those obtained by other researchers.

Based on the wind tunnel tests, it can be concluded that the lift to drag ratio for the morphed configuration is greater for higher lift coefficient. At Reynolds number 293000, C_L/C_D for the morphed configuration is higher for lift coefficient greater than 0.7 and the $(C_L/C_D)_{max}$ is also higher than that of the original configuration. This proves that the employment of SMA actuators in the wing model, combined with the use of flexible skin may improve flight performance. The SMA actuators can be switched on and off depending on the velocity and angle of attack, in order to obtain better lift to drag ratio.

References

[1] Roskam, J. and Lan, C. T. E. *Airplane Aerodynamics and Performance*. DARcorporation, 2000.

[2] Bolonkin, A. and Gilyard, G. B. Estimated Benefits of Variable-Geometry Wing Camber Control for Transport Aircraft. *NASA TM 1999-206586*, 1999.

[3] Dong, Y., Boming, Z., and Jun, L. A Changeable Aerofoil Actuated by Shape Memory Alloy Springs. *Materials Science and Engineering A*, Vol. 485, 2008, pp. 243–250.

[4] Hutapea, P., Kim, J., Guion, A., Hanna, C., and Heulitt, N. Development of a Smart Wing. *Aircraft Engineering and Aerospace Technology: An International Journal*, Vol. 80, No. 4, 2008, pp. 439–444.

[5] Popov, A. V., Labib, M., Fays, J. and Botez, R. M. Closed-Loop Control Simulations on a Morphing Wing. *Journal of Aircraft*, Vol. 45, No. 5, 2008, pp. 1794-1803.

[6] Strelec, J. K., Lagoudas, D.C., Khan, M. A., and Yen, J. Design and Implementation of a Shape Memory Alloy Actuated Reconfigurable Wing. *Journal of Intelligent Material Systems and Structures*, Vol. 14, 2003, pp. 257-273.

[7] Culshaw, B. *Smart Structures and Materials*. Artech House, Inc., Boston, 1996.

[8] Fontanazza, F., Talling, R., Jackson, M., Dashwood, R., Dye D., and Iannucci, L. Morphing Wing Technologies Research. *Seas DTC First Conference*, 2006.

[9] Bar-Cohen, E. *Electroactive Polymer (EAP) Actuators as Artificial Muscles: Reality, Potential, and Challenges*. 2nd Edition Vol. PM136, SPIE Press, Bellingham, WA, 2004.

[10] Nishiyama, Z. *Martensitic Transformations*. Academic Press, San Diego, CA, 1978.

[11] Kaufman, L., and Cohen, M. Martensitic Transformations. *Progress in Metal Physics*, Vol. 7, 1958, pp. 165-246.

[12] McCroskey, W. J. A Critical Assessment of Wind Tunnel Results for the NACA0012 Airfoil. NASA Technical Memorandum 10001 9 USAAVSCOM Technical Report 87-A-5, 1987.

[13] Alam, F, Zimmer, G, and Watkins, S. Mean and time-varying flow measurements on the surface of a family of idealized road vehicles. *Journal of Experimental Thermal and Fluid Sciences* Vol. 27, No. 5, 2003, pp. 639–654.

[14] Goraj,Z., Frydrychewicz, A., Świtkiewicz, R., Hernik, B., Gadomski, J., Goetzendorf-Grabowski, T., Figat, M., Suchodolski, St. and Chajec W. High Altitude Long Endurance Unmanned Aerial Vehicle of a New Generation – A Design Challenge for a Low Cost, Reliable and High Performance Aircraft. *Bulletin Of The Polish Academy Of Sciences, Technical Sciences*, Vol. 52, No. 3, pp. 173-194, 2004.

7 Contact Author Email Address

The author can be contacted at ermira.abdullah@student.rmit.edu.au.

Copyright Statement